Journal of Alloys and Compounds 518 (2012) 27–31

Contents lists available at SciVerse ScienceDirect

Journal of Alloys and Compounds

journal homepage: www.elsevier.com/locate/jallcom

Master sintering curve of nanocomposite WC-MgO powder compacts

C.X. Ouyang[a,b], S.G. Zhu[a,b,c,*], J. Ma[a,b], H.X. Qu[b,c]

[a] College of Mechanical Engineering, Donghua University, Shanghai 201620, PR China
[b] College of Material Science and Engineering, Donghua University, Shanghai 201620, PR China
[c] Engineering Research Center of Advanced Textile Machinery, Ministry of Education, Shanghai 201620, PR China

ARTICLE INFO

Article history:
Received 17 October 2011
Received in revised form
15 December 2011
Accepted 19 December 2011
Available online 27 December 2011

Keywords:
Master sintering curve
WC
MgO
Densification evolution

ABSTRACT

The master sintering curve (MSC) of nanocomposite WC-MgO was constructed based on the combined-stage sintering model. Nano-sized WC-4.3wt%MgO powder with an average particle size of 35 nm was synthesized by high-energy ball milling and then pressed uniaxially at a pressure of 500 MPa to fabricate green compacts. The shrinkage response of the compacts during heating was studied by dilatometric runs at constant heating rates of 5 and 10 °C/min up to 1900 °C. The master sintering curve with sintering activation energy Q = 361.8 kJ/mol was constructed between 600 and 1900 °C. The MSC was validated by isothermal and non-isothermal sintering experiments with identical green compacts. The results demonstrate that the MSC can be successfully applied to predict and control densification evolution during heating, regardless of the heating path, and non-isothermal sintering in the high-temperature range.

1. Introduction

Amongst hard alloys, tungsten carbide (WC) incorporating binding materials (Co, Fe or Ni) has attracted significant scientific and technological attention for use cutting tools, drilling and mining equipment. A metallic binder (mainly Co) is added to offset the characteristic brittle behavior of the WC ceramic and increase the compact toughness [1,2]. However, metallic binders result in poor corrosion/oxidation resistance, environmental toxicity and high-cost [3]. Therefore, efforts to obtain harder materials have attempted to consolidate WC with low amounts of cobalt or without metal binder.

During the past few decades, some research efforts have focused on the consolidation of a WC matrix reinforced by a secondary phase [4,5]. This ceramic/ceramic can be prepared through a relatively inexpensive and simple process. Among these, a new composite, WC-MgO, is considered to be an ideal material for use in industrial practice, due to its combination of superior hardness and toughness [6,7]. There has been research on the synthesis of WC-MgO composite powders via mechanical alloying but less on the sintering details.

Solid state sintering has been recognized as a very complex process, involving the evolution of microstructure through the action of several transport mechanisms. Su and Johnson developed the master sintering curve (MSC) concept to predict the densification behavior using a minimum of preliminary experiments [8]. The formulation and construction of MSC is derived from combined-stage sintering [9], which extends the analysis of sintering beyond the confined segments described by individual stage models. The instantaneous linear shrinkage rate in this model is given as:

$$-\frac{dL}{Ldt} = \frac{\gamma\Omega}{kT}\left(\frac{\Gamma_v D_v}{G^3} + \frac{\Gamma_b \delta D_b}{G^4}\right) \quad (1)$$

where γ is the surface energy, Ω is the atomic volume, k is the Boltzmann constant, L is the length of sample, T is the absolute temperature, t is the time, G is the mean grain diameter, D_v and D_b are the coefficients for volume and grain boundary diffusion, δ is the thickness of the region of enhanced diffusion at the grain boundary, Γ_v and Γ_b are the lumped geometric scaling parameters for volume and grain boundary diffusion, respectively. For isotropic shrinkage, the linear shrinkage rate can be converted to the densification rate by

$$-\frac{dL}{Ldt} = \frac{d\rho}{3\rho dt} \quad (2)$$

where ρ is the bulk density. Assuming that densification during sintering is thermally activated and controlled by a single dominant diffusion mechanism (either volume or grain boundary diffusion) and assuming that G, Γ_b and the microstructure evolution are

* Corresponding author at: College of Mechanical Engineering, Donghua University, Shanghai 201620, PR China. Tel.: +86 21 6779 2813; fax: +86 21 6779 2813.
E-mail address: sgzhu@dhu.edu.cn (S.G. Zhu).

0925-8388/$ – see front matter.
doi:10.1016/j.jallcom.2011.12.091

dependent only on density. Then Eq. (1) rearranges and simplifies to

$$\int_{\rho_0}^{\rho} \frac{(G(\rho))^n}{3\rho\Gamma(\rho)}\, d\rho = \int_0^t \frac{\gamma\Omega D_0}{kT} \exp\left(-\frac{Q}{RT}\right) dt \quad (3)$$

where D_0 is the diffusion coefficient for the dominant diffusion mechanism, Q is the apparent activation energy for sintering, n is a constant depend on the diffusion mechanism and R is the gas constant. The left-hand of this equation depends on the microstructural evolution and materials properties:

$$\Phi(\rho) \equiv \frac{k}{\gamma\Omega D_0} \int_{\rho_0}^{\rho} \frac{(G(\rho))^n}{3\rho\Gamma(\rho)}\, d\rho \quad (4)$$

The right-hand of Eq. (3) depends on the Q and the time-temperature profile:

$$\Theta(t, T(t)) \equiv \int_0^t \frac{1}{T} \exp\left(-\frac{Q}{RT}\right) dt \quad (5)$$

The relationship between ρ and $\Theta(t, T(t))$ is defined as the master sintering curve. The MSC is unique for a given powder and green-body process. This theory, originally developed and demonstrated for solid state sintering that exhibits isotropic behavior, has been successfully applied to the solid state sintering of nano-CeO_2 [10], nano-sized ZnO [11], Al_2O_3-8 mol%YSZ [12], TiO_2 [13], nano-3Y-TZP [14] and ZrO_2 [15]. However, the application of MSC to the sintering of WC-MgO compacts has not been reported. The present work was aimed at establishing a master sintering curve for nanocomposite WC-MgO powder compacts and to demonstrate how the theory can be applied to design a reproducible process for fabricating a controlled density.

2. Experimental

To produce nanocrystalline WC-4.3wt%MgO via mechanical alloying process in a QM-1SP4 high-energy planetary ball milling machine, WC powder (99.5% purity, 75 μm) and MgO (98.5% purity, 48 μm) were used in this study. The ball mill process was carried out under argon gas atmosphere at a rotational speed of 350 revolutions per minute (rpm) for 50 h. The mill balls (10 mm diameter) and vial were made of cemented carbides materials. The ball-to-powder weight ratio was 10:1.

The morphologies of the as-milled powders were investigated by transmission electron microscope (TEM) on a JEOL JEM-2100F electron microscope. The specific surface area of the powders was determined using a Brunauer–Emmett–Teller (BET) surface area analyzer (Autosorb-1, Quantachrome, United States). The particle size of the powders was measured by dynamic laser light scattering method (DLLS, BI-200SM, Brookhaven, United States).

Powders were pressed using a uniaxial pressure of 500 MPa to create bars of 5 mm × 5 mm × 25 mm. The green density of the compacts measured by the geometric method was 50.37 ± 0.3% of the theoretical density. The linear shrinkage were monitored in a dilatometer (DIL 402C, Netzsch) heated to 1900 °C from room temperature with an argon flow at 50 ml/min. Constant heating rates (HRs) of 5 and 10 °C/min were used. To ensure experimental consistency, typically three samples were characterized at each heating rate. The accuracy of the measurement was found to be within ±0.1 μm.

The ability to use the MSC to predict and control the sintering process was assessed by designing two different sintering schedules under a consistent sintering condition using a high-temperature laboratory furnace as follows: (I) For non-isothermal sintering, ten green compacts were heated up to reach a desired temperature at constant heating rates of 2, 5, 10 and 15 °C/min without a holding time and cooling down naturally; (II) isothermal sintering experiments were carried out at temperatures of 1400, 1550 and 1700 °C with holding dwell times of 3, 10, 30, 60, 90 or 120 min. All of the green samples were fabricated using the same source powder and compaction process. The density of the specimens after sintering was determined from the measured sample dimensions and mass and by using the Archimedes liquid immersion technique.

3. Results and discussion

3.1. Powder characterization

Fig. 1 shows the morphology of the as-milled WC-MgO composite powder. In the figure, the particles have a size range of 10–50 nm and mainly exhibit irregular polygonal shapes. Using DLLS, the median particle size (D50 value) of the nanocomposite powder was 35 nm. The results of the BET test indicated the effect of ball milling on the surface area of the powders revealing a nearly 60.3% increment in the surface area of the powder from 11.6 to 18.6 $m^2\,g^{-1}$ during the milling process.

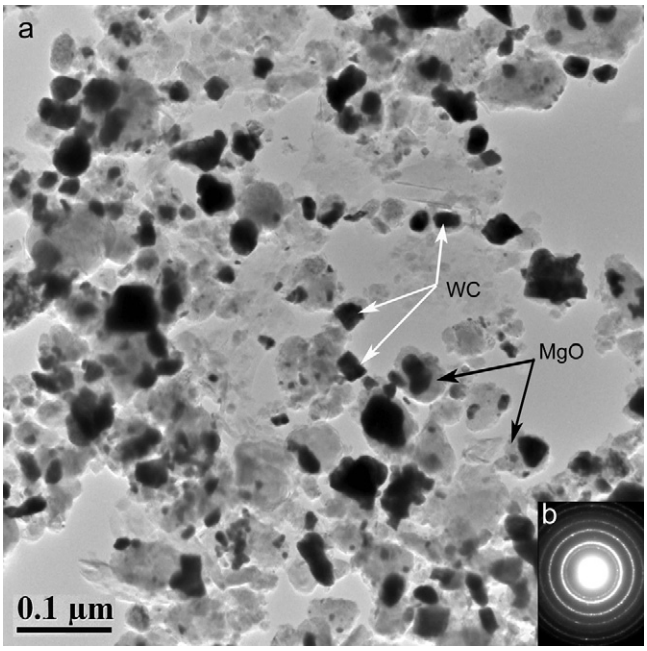

Fig. 1. Transmission electron micrograph and selected area diffraction pattern of nanocomposite WC-MgO powders after 50 h of the ball-milling time.

3.2. Dilatometry and construction of MSC

Fig. 2 shows the dL/L_0 versus temperature curves under heating rates of 5 and 10 °C/min. It can be observed from the figure that the onset of the shrinkage process started around at 780 °C in both runs. For each heating rate, the shrinkage rate increased to a maximum and then decreased. The heating rate was found to have little influence on the final shrinkage, because all the samples achieved the maximum level of shrinkage (19% of L_0 at 1880 °C).

In the temperature range 1100 to 1500 °C, the higher heating rate caused less shrinkage than the lower heating rate, because

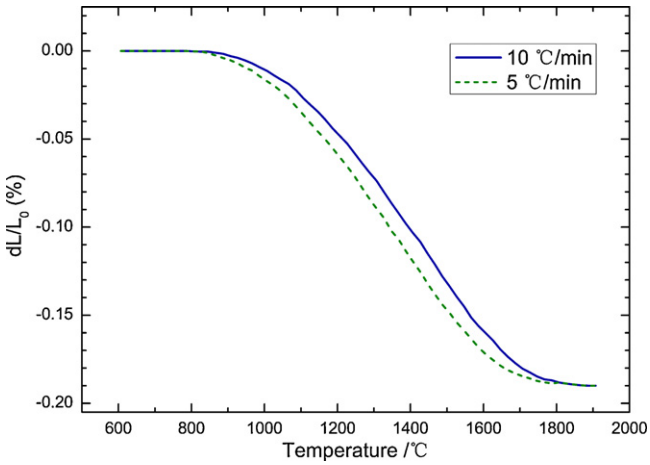

Fig. 2. Dilatometric curves of WC-MgO compacts under heating rates of 5 °C/min and 10 °C/min.

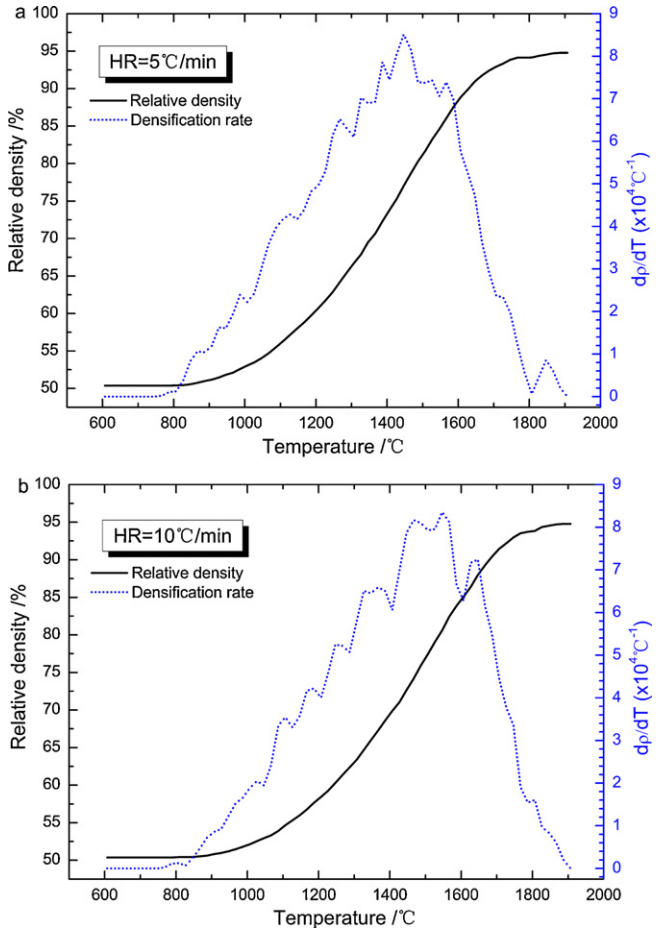

Fig. 3. Relative density and densification rate as a function of sintering temperature under heating rates of 5 °C/min (a) and 10 °C/min (b).

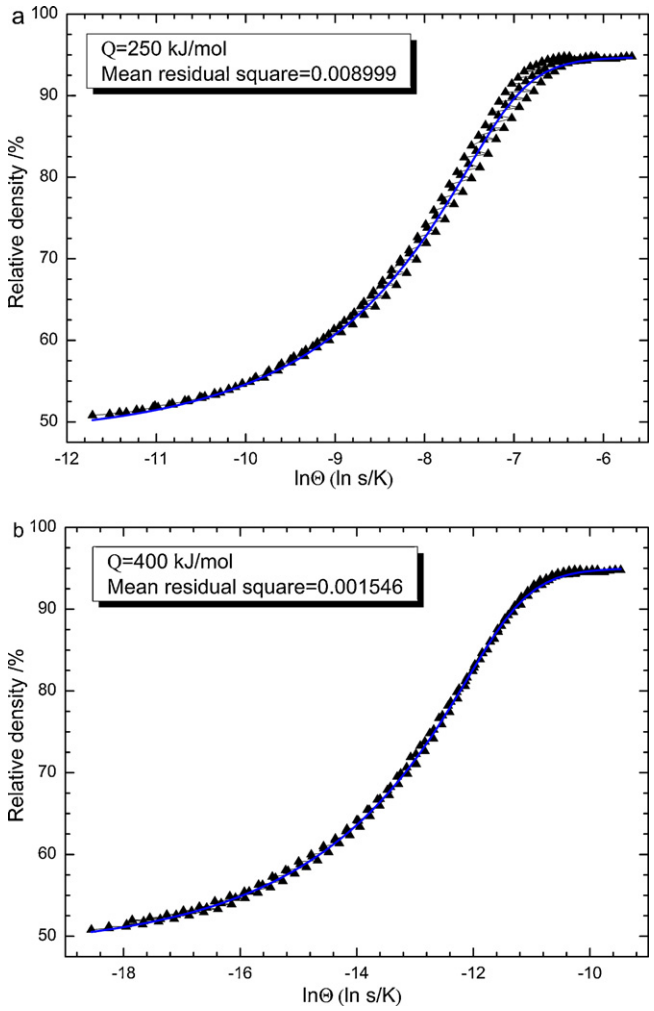

Fig. 4. Construction of master sintering curves for WC-MgO compacts at activation energy of 250 kJ/mol (a) and 400 kJ/mol (b).

the green compact was exposed to sintering for a longer time at 5 °C/min. It is noted that this behavior has also been observed in dilatometric experiments for nano-sized ZnO [11], nano-3Y-TZP [14], ZrO_2 [15] and can be ascribed to the shortened time for diffusion and mass transport when a higher heating rate is used to reach a given temperature.

The density and densification rate versus temperature can be converted from the dilatometric curves using Eq. (6)

$$\rho = \left(\frac{1}{(1 - dL/L_0)^3}\right)\rho_0 \tag{6}$$

where ρ and ρ_0 are the density of sintered and green compacts, L_0 is the initial length of the compact, and dL/L_0 is the instantaneous linear shrinkage. In Fig. 3, the density versus temperature exhibits the familiar sigmoidal shape regardless of heating history. Densities show a modest but systematic dependence on heating rate and the final density is 94.78(%TD). Under the heating rate of 10 °C/min, the densification rate approached a maximum value when the temperature reached 1540 °C whereas the maximum shrinkage rate moved to a lower temperature (1440 °C) under the heating rate of 5 °C/min.

As mentioned earlier, the activation energy for densification is a characteristic quantity that elucidates the fundamental diffusion mechanisms during the sintering process. It is also one of the important parameters for obtaining a master sintering curve. In the construction of the MSC, an optimum value of apparent activation energy in Eq. (5) is determined and the $\rho - \Theta(t,T(t))$ trajectory is constructed for different heating profiles. The $\rho - \Theta(t,T(t))$ data are fitted to a sigmoidal (S-shape) curve [16,17], defined as follows,

$$\rho = \rho_0 + \frac{100 - \rho_0}{1 + \exp(-\log(\Theta) - a/b)} \tag{7}$$

where a and b are constants defining the sigmoid curve, and ρ_0 is the green density.

Accordingly, if the activation energy (Q) is unknown, it can be estimated from the Θ vs ρ data. If the correct value of Q has been estimated, all data points should fall on a single sigmoidal curve. As examples, Fig. 4 shows the MSC curves constructed at Q = 250 and 400 kJ/mol. In both cases, it is difficult to establish a good fit for the $\ln(\Theta) - \rho$ data points under different heating rates with the given value of activation energy. In addition, if the data points cannot converge, a new Q is chosen and the above steps are iterated until the particulate value is decided. In the fitting process, the minimum average residual square is calculated by Eq. (8).

$$\text{Mean residual} = \sqrt{\frac{1}{\rho_f - \rho_0}\int_{\rho_0}^{\rho_f} \frac{\sum_{i=1}^{N}\left((\Theta_i/\Theta_{i\_avg}) - 1\right)^2}{N}\, d\rho} \tag{8}$$

where ρ_f is the final relative density, N is the total number of experimental data, i is the dummy variable for summation, Θ_i is the work of sintering at ith value of density, and Θ_{i_avg} is the average value of work of sintering at ith value of density, respectively.

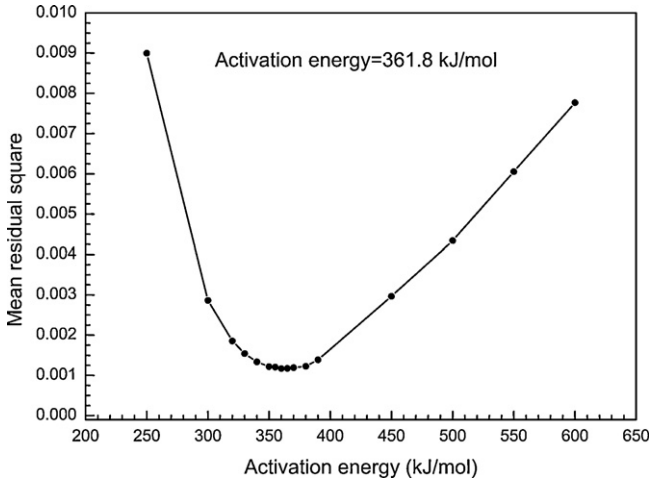

Fig. 5. Mean residual squares for the various values of the activation energy.

The best convergence occurs at $Q = 361.8$ kJ/mol, with a minimum mean residual square (0.001171) found from Fig. 5, which gives the mean residual squares for various given values of activation energy. Hence, the MSC is constructed under an apparent activation energy $Q = 361.8$ kJ/mol as shown in Fig. 6.

3.3. Validation and prediction of MSC

Before applying the constructed master sintering curve to industrial practice, the validity of the MSC should be verified through a sufficient amount of isothermal and non-isothermal sintering experiments. In Fig. 7, the relative densities of sintered samples were determined by Archimedes method. The densities of ten sintering cycles selected randomly under heating rates of 2, 5, 10 and 15 °C/min are shown in Table 1. The non-isothermal experimental results show good agreement with densities predicted from the MSC. The small errors would be caused by the fact that the calculated density values converted from dilatometric runs were monitored at a specific temperature, while the densities measured by the Archimedes method were tested at room temperature. It is shown that the density profile versus time-temperature integral could be a promising and practical approach used to predict the final density sintered at a given temperature, irrespective of the heating path.

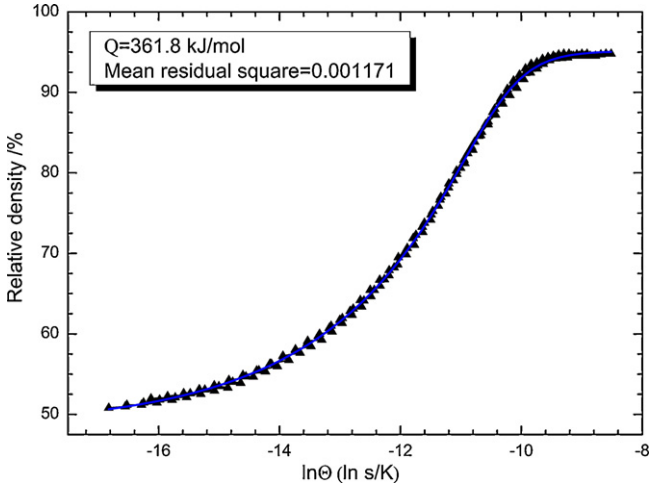

Fig. 6. Construction of MSC for WC-MgO compacts using an activation energy of 361.8 kJ/mol.

Table 1
Relative densities of sintered samples under different heating paths determined by Archimedes method.

Samples no	Heating paths	Relative density/%
1	15 °C/min to 1900 °C	94.99 ± 1.19
2	10 °C/min to 1850 °C	93.70 ± 1.37
3	5 °C/min to 1700 °C	90.79 ± 1.19
4	2 °C/min to 1550 °C	87.20 ± 1.27
5	2 °C/min to 1450 °C	81.19 ± 1.21
6	10 °C/min to 1500 °C	75.39 ± 1.15
7	5 °C/min to 1400 °C	73.79 ± 1.19
8	15 °C/min to 1500 °C	69.40 ± 1.18
9	15 °C/min to 1450 °C	65.10 ± 1.25
10	2 °C/min to 1200 °C	63.39 ± 1.33

Fig. 8 shows the response surface for the sintering time required to reach a desired density under a constant holding temperature, obtained from Eq. (5) and $Q = 361.8$ kJ/mol. It can be clearly observed that the required holding time to reach the desired density at high temperature is much shorter than at low temperature. As examples, the holding time was 5 min when sintering at 1700 °C to attain a bulk density of 90%TD, the holding time was 105 min at 1500 °C to reach the same level, and the predicted result of holding time is 175 h for isothermal experiments at 1200 °C.

However, the predicted data do not fit very well with the experimental results at lower temperature, as demonstrated in Fig. 9. Note that the activation energy determined by the MSC method is for the combined sintering stage, i.e. the calculated sintering activation energy for densification takes into account all the combined effects of surface, grain boundary and volume diffusion [9]. Also, the activation energy for surface diffusion is smaller than that required for either grain-boundary or volume diffusion [8]. With increasing holding time at 1400 °C, the deviation of the experimental data from the predicted data becomes marked, owing to dominance of the surface diffusion mechanism during the initial stage of solid-stage sintering [13]. This is also observed during the two-step sintering of WC-MgO compacts [6]. In Fig. 9, the densities of the isothermal experiments at 1700 and 1550 °C are in better agreement with the curve than for low-temperature runs, because either volume or grain boundary diffusion dominate when at higher temperature [8]. Overall, in the high-temperature range, predictions can be made for virtually any combination of sintering time and temperature with the help of the constructed MSC.

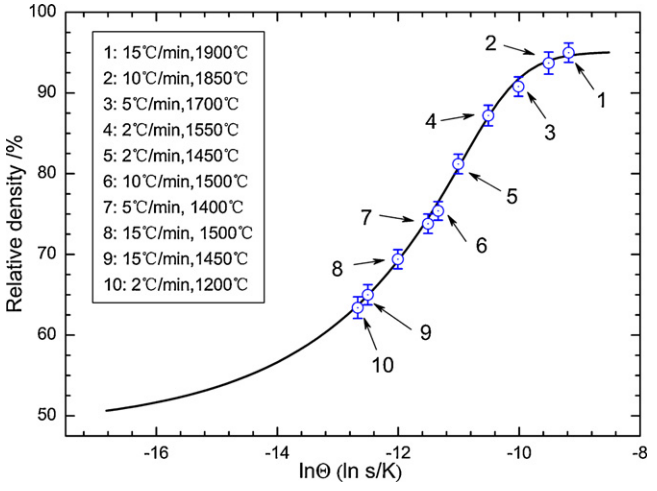

Fig. 7. Validation of master sintering curve for WC-MgO compacts. The non-isothermal experimental results of ten sintering cycles agreed well with the predicted curve.

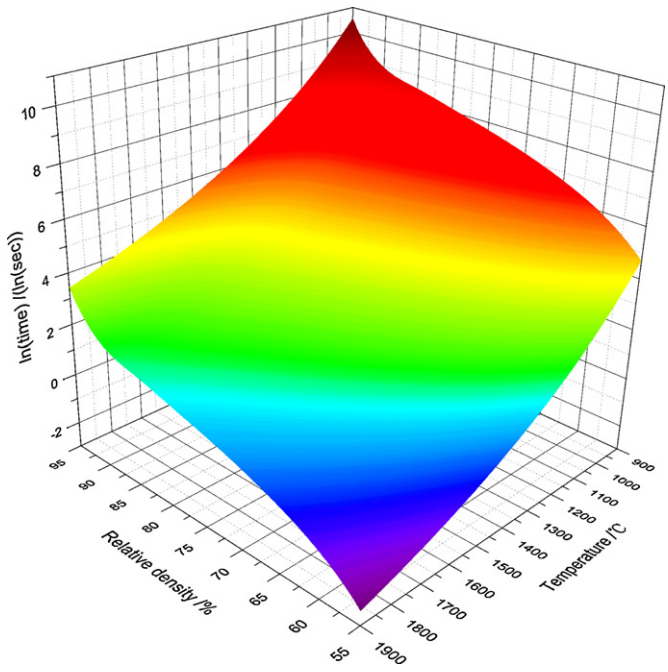

Fig. 8. The predictions of the sintering time (ln(sec)) required for WC-MgO compacts to reach a particular density at a constant temperature.

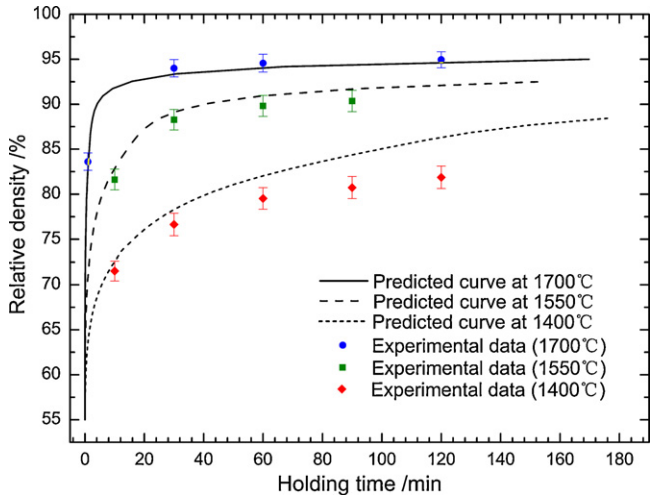

Fig. 9. Comparison of the predicted densification results with the experimental results (isothermal sintering runs at 1400 °C, 1550 °C and 1700 °C).

4. Conclusions

In this work, a master sintering curve based on the combined-stage sintering model has been applied to the consolidation of a WC-4.3 wt%MgO nanocomposite. The sintering activation energy was estimated to be 361.8 kJ/mol, using the minimum residual square. The ability of MSC models to predict and control the sintering process for identical WC-MgO compacts was verified by non-isothermal and isothermal experiments under the same sintering conditions. The experimental results for non-isothermal and isothermal processes at high temperature agreed well with the predicted curves. The obvious deviation of isothermals was caused by the domination by surface diffusion rather than volume diffusion or grain-boundary diffusion mechanisms at the low-temperature range.

Acknowledgements

The authors would like to acknowledge the financial support provided by Shanghai Leading Academic Discipline Project under Project No: B602, and the support by the Nanomaterials Research Special Foundation of Shanghai Science and Technology Committee under Grant No: 05nm05031.

References

[1] M.S. El-Eskandarany, A.A. Mahday, H.A. Ahmend, A.H. Amer, J. Alloys Compd. 312 (2000) 315–325.
[2] Z.Z. Fang, X. Wang, T. Ryu, K.S. Hwang, H.Y. Sohn, Int. J. Refract. Met. Hard Mater. 27 (2009) 288–299.
[3] S. Hochstrasser, Y. Mueller, C. Latkoczy, S. Virtanen, P. Schmutz, Corros. Sci. 49 (2007) 2002–2020.
[4] O. Malek, B. Lauwers, Y. Perez, P.D. Baets, J. Vleugels, J. Eur. Ceram. Soc. 29 (2009) 3371–3378.
[5] M.S. El-Eskandarany, J. Alloys Compd. 296 (2000) 175–182.
[6] J. Ma, S.G. Zhu, C.X. Ouyang, J. Eur. Ceram. Soc. 31 (2011) 1927–1935.
[7] C.X. Wu, S.G. Zhu, J. Ma, M.L. Zhang, J. Alloys Compd. 478 (2009) 615–619.
[8] H. Su, D.L. Johnson, J. Am. Ceram. Soc. 79 (1996) 3211–3217.
[9] J. Hansen, R.P. Rusin, M.H. Teng, D.L. Johnson, J. Am. Ceram. Soc. 75 (1992) 1129–1135.
[10] Y. Kinemuchi, K. Watari, J. Eur. Ceram. Soc. 28 (2008) 2019–2024.
[11] K.G. Ewsuk, D.T. Ellerby, C.B. Diantonio, J. Am. Ceram. Soc. 89 (2006) 2003–2009.
[12] X.C. Song, J. Lu, T.S. Zhang, J. Ma, J. Am. Ceram. Soc. 94 (2011) 1053–1059.
[13] D. Li, W.Q. Chen, X.H. Shao, Y.H. Ge, Y.C. Zhang, S.S. Zhang, Mater. Lett. 62 (2008) 849–851.
[14] M. Mazaheri, A. Simchi, M. Dourandish, F. Golestani-Fard, Ceram. Int. 35 (2009) 547–554.
[15] R. Caruso, N. Mamana, E. Benavidez, J. Alloys Compd. 495 (2010) 570–573.
[16] D.C. Blaine, S.J. Park, R.M. German, J. Am. Ceram. Soc. 92 (2009) 1403–1409.
[17] M.H. Teng, Y.C. Lai, Y.T. Chen, Western Pacific Earth Sci. 2 (2002) 171–180.